Journal of Non-Crystalline Solids 354 (2008) 5521–5528

Contents lists available at ScienceDirect

Journal of Non-Crystalline Solids

journal homepage: www.elsevier.com/locate/jnoncrysol

Octahedral fluoride glasses: Raman spectra and structure of niobium pentafluoride

G.N. Papatheodorou [a,*], A.G. Kalampounias [b], S.N. Yannopoulos [a]

[a] Foundation for Research and Technology Hellas – Institute of Chemical Engineering and High Temperature Chemical Processes, FORTH-ICE/HT, P.O. Box 1414, GR-26 504, Patras, Greece

[b] Department of Chemical Engineering, University of Patras, GR-26 504, Patras, Greece

ARTICLE INFO

Article history:
Received 21 January 2008
Available online 14 September 2008

PACS:
64.70.Pf
61.43.Fs
63.50.+x
62.60.+v

Keywords:
Raman scattering
Fluorides
Halide glasses
Structure
Long-range order
Short-range order
Glass transition
Fragility

ABSTRACT

Raman spectroscopy is used to characterize the NbF_5 phases in the temperature range 80–500 K. A new clear glass is formed by quenching the melt to liquid nitrogen temperatures having a glass transition at ~206 K and crystallization at ~233 K. For all phases including the melt, the glass, the supercooled liquid, the crystalline solid and the gas, the Raman spectra show a rather common high frequency band at ~760 cm^{-1} which is attributed to the Nb–F terminal frequency of partially bridged 'NbF_6' octahedra. Based on the systematics of the Raman spectra for all phases and the literature physicochemical data a model is proposed for the glass and the liquid phases where 'NbF_6' octahedral bridged in *cis* and/or *trans* configurations form a variety of cyclic and/or chain structures which intermix building up the overall structure. At exceptionally low energies (<11 cm^{-1}) a rather weak in intensity Boson peak is observed in the glass which shifts to even lower energies with increasing temperature. Librational and/or tortional motions of the bridged octahedra participating in the glass structure are possible candidates for the origin of this peak.

1. Introduction

Metal halide glasses are usually formed by quenching the corresponding melts to room temperature. Typical examples are certain fluorides used as components of ZBLAN [1,2] as well as the zinc halides and their mixtures [3]. In a series of experiments conducted in our laboratory we have found that a large number of simple low melting (T_m < 600 K) metal halide inorganic salts have a tendency to form glasses upon quenching the melt into liquid nitrogen (LN_2) temperatures. Such behavior has been reported in conference publications for the NbF_5 and TaF_5 [4], but preliminary work has shown that the glass formation is more general for other MF_5 (M = Mo, Sb, etc.) salts as well as for metal halide 'adduct' salts like $AlX_3 \cdot NH_3$ (X = Cl, Br) [5].

The present work concerns with the structural investigation of the different 'phases' observed in NbF_5 from the quenched glass at LN_2 temperatures up to the high temperature melt at 500 K. Raman spectroscopy is used for studying the structural changes and correlations between the molten, glassy and crystalline phases of NbF_5. Special attention is given to the purity of the salt used and for accurately measuring the sample temperature. Based on the Raman spectroscopy measurements and the physicochemical properties of NbF_5 a structural model is proposed for the molten and glassy states. Furthermore, the glass transition (T_g) and crystallization temperatures (T^*_{cr}) are estimated from the Raman spectral changes with temperature. Finally, the characteristic for most glasses Boson peak is seen in the low frequency region of the spectra and its temperature dependence is documented and discussed in terms of its physical origin.

2. Experimental

The starting material for preparing high purity NbF_5 was purchased from Alfa-Johnson Matthey as 99.9% pure. Repeated slow sublimations of the commercial material in sealed fused silica tubes gave crystalline NbF_5 which was further used for preparing the liquid and glass phase. The handling of NbF_5 and the filling of the Raman cells took place in a controlled argon atmosphere glove box with a water content of less than 1 ppm. Fused silica tubes, previously degassed at temperatures ~1000 °C under vacuum, were used for both storing NbF_5 in the glove box and for making the Raman cells.

* Corresponding author.
E-mail address: gpap@iceht.forth.gr (G.N. Papatheodorou).

0022-3093/$ - see front matter © 2008 Elsevier B.V. All rights reserved.
doi:10.1016/j.jnoncrysol.2008.08.005

The Raman setup, the optical furnace and the procedures for measuring spectra at elevated temperatures have been described elsewhere [3]. For the low temperature spectral measurements a liquid-nitrogen-cooled pyrex glass optical 'Dewar type' cryostat was constructed. Within the cryostat a copper metal cylindrical block (10 mm diameter; 4 cm long) with optical opening was used as sample holder. The cylindrical block was wound with insulated ARi wire (Ari Industries Inc., Illinois) resistance allowing temperature variation and control in the temperature range 80–290 K. A 'CAL' temperature controller was used which allowed measurements with accuracy ±0.2 K. The Raman cells were made from fused silica tubing (4 mm outer diameter, 3 mm inner diameter, ~2 cm long) and were placed either in an appropriate opening (~4.1 mm diameter) inside the cooled copper block or in the high temperature furnace.

A series of visual experiments were first carried out showing the existing phases of NbF_5. A Raman cell containing crystalline NbF_5 was heated to ~50 K above its melting point (325 K) and was then quenched into liquid nitrogen. The melt was solidified forming a transparent glass possessing a well-defined long negative meniscus due to volume contraction. Warming the glass outside the liquid nitrogen resulted slowly in the disappearance of the meniscus and the formation of a rather fluid supercooled liquid (s.l.) which was crystallized with further heating. In order to estimate the volume difference between the glass and the s.l. the Raman cell was quickly photographed under magnification when the material was in either the glassy or the s.l. phase. A detailed comparison between these two pictures allowed the estimation (with an error of ±10%) of the percentage volume change at the glass transition. Furthermore, the same method was used in order to estimate the volume difference between the s.l. at ~300 K and the regular liquid (melt) at ~350 K. The transformation range of the glass transition was also estimated by placing the Raman cell containing the quenched glass, into the cryostat and by observing the meniscus changes with temperature variation. By further increasing the temperature of the Raman cell the s.l. was crystallized (exothermically). The solid melted at 325 K giving a rather fluid melt which could be supercooled to ~300 K without crystallization.

The procedures for measuring the Raman spectra of the various phases were the following: the Raman cell was heated above melting and after quenching into liquid nitrogen was quickly placed inside the cold copper block of the cryostat at ~80 K. The temperature was then raised slowly and Raman spectra were measured in 5 K steps. Smaller steps of ~1 K were used for measuring the spectra around the phase transition temperatures. At room temperature the cell was transferred into an optical furnace for further increasing the temperature and measuring the melt spectra up to 500 K.

Raman spectra of the amorphous phases were measured at right angle in both the polarized (VV: vertical polarization of incident laser – vertical analysis of scattered light) and the depolarized (VH: vertical polarization of incident laser – horizontal analysis of scattered light) scattering geometries in the spectral region 5–900 cm^{-1}. No polarization measurements were conducted in the crystalline state due to its polycrystalline character. Following the methods described in [6] the VV and VH spectra were used for calculating the reduced Raman spectra R_{VV} and R_{VH} as well as the isotropic (ISO) and anisotropic (ANISO) representations.

3. Results

3.1. Characterization of the amorphous phase

Both the Raman measurements and the visual experiments have indicated that a series of phase transitions occur by heating the NbF_5 glass formed by quenching the melt from about 400 K to LN_2 temperatures. The procedures followed and the phases observed are shown in the diagram.

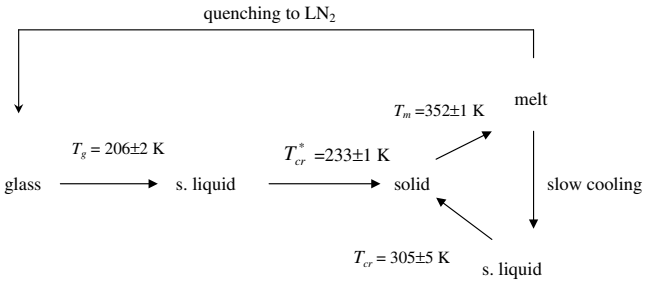

Thus, by slow cooling the melt a supercooled liquid (s.l.) is formed which crystallizes at ~305 K. The supercooled state is also accessible by heating the glass above T_g. This metastable liquid phase crystallizes exothermically at T^*_{cr}. The determination of T^*_{cr} and T_g is described below while the T_m and T_{cr} were estimated by placing the Raman cell in a variable temperature optical furnace with a thermocouple next to the sample and visually observing the phase transition. The fact that the low temperature s.l. becomes quite fluid over a very short temperature range just above T_g points to a very fragile nature of this supercooled liquid.

The Raman spectra of all the possible phases of NbF_5, shown in the above diagram, are illustrated in Fig. 1. The upper spectrum in Fig. 1, taken from Ref. [7], is that of the NbF_5 gas which exhibits a dimer (D)–monomer (M) equilibrium. The low frequency region of all non-crystalline phases was examined carefully. The temperature dependent VV spectra for the glass at low temperatures (below

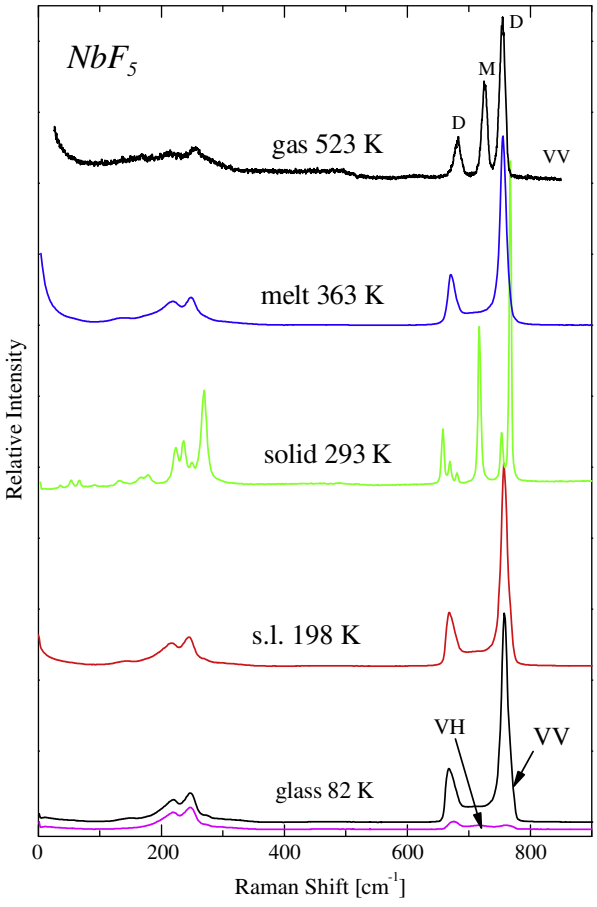

Fig. 1. Raman spectra of NbF_5 phases obtained upon heating the quenched glass. Spectral conditions: laser line = 514.5 nm; power = 20–100 mW; resolution = 1.5 cm^{-1}. The gas phase spectra are from Ref. [7].

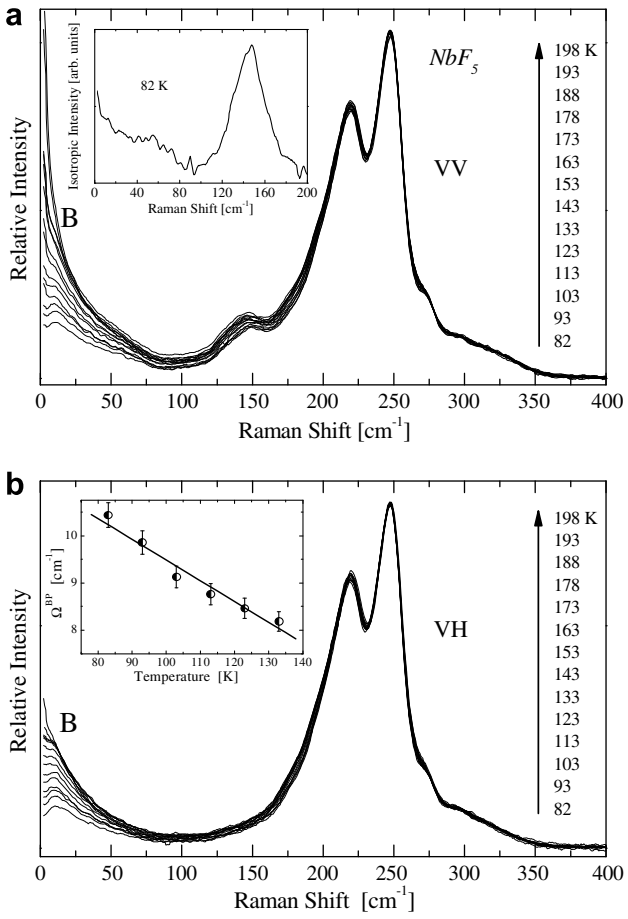

Fig. 2. Polarized (a) and depolarized (b) Raman spectra in the low frequency region of the glass and the supercooled liquid for selected temperatures as shown in the legends. The spectra were normalized with respect to the peak intensity at 250 cm^{-1}. B denotes the Boson peak region. Spectral conditions as in Fig. 1. Inset in (a): expanded isotropic low temperature, low frequency spectrum. Inset (b): temperature dependence of the Boson peak energy, see Section 4.2 for details.

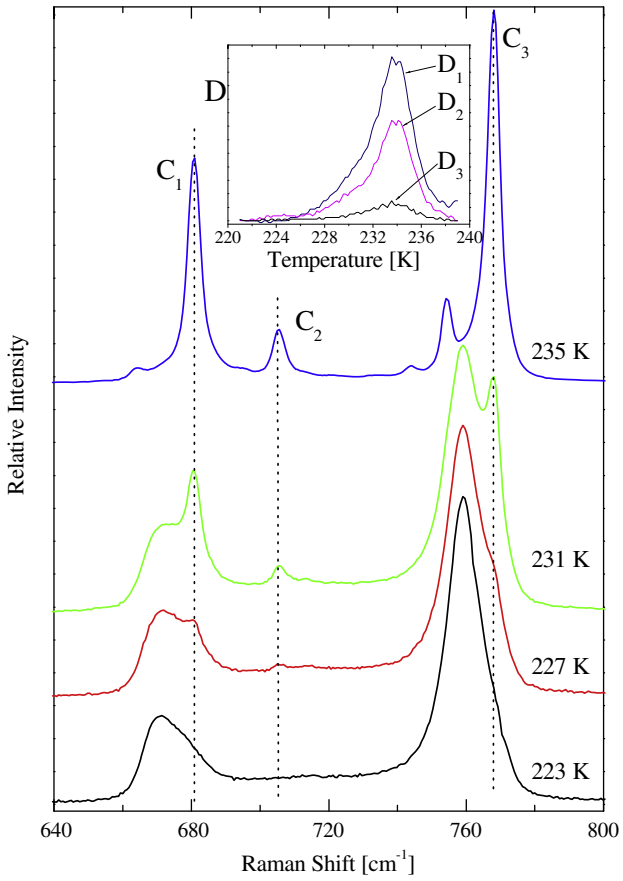

Fig. 3. Selected Raman spectra near the glass crystallization temperature. Bands due to the crystalline phase (marked as C_1, C_2 and C_3) start appearing at ~225 K. Inset: the temperature derivative $\left(D_i = \frac{dI_{C_i}}{dT}\right)$ of the intensity of the C_i band (I_{C_i}) relatively to glass band intensity at ~760 cm^{-1}. Spectral conditions as in Fig. 1.

T_g) are shown in Fig. 2 revealing the characteristic Boson peak. At higher temperatures the Boson peak is overwhelmed by the 'liquid' Rayleigh wing and cannot be seen in the supercooled liquid.

At this point it should be pointed out that in an earlier preliminary report [4] there were indications that the crystallization of the s.l. lead to two consecutive crystalline allotropic forms of NbF_5. In contrast, the present measurements showed that only one solid, the well known monoclinic NbF_5 [8,9] is formed during the above cycle. No other crystalline allotrope could be detected with the Raman experiments by either slow or fast heating of the s.l. This difference lies likely on the fact that the NbF_5 was better purified in the present work using repeated slow sublimations. Furthermore, all containers and cells were made from fused silica tubing which has been thoroughly degassed before use. As it was recently shown for $ZnCl_2$ small amounts of moisture or oxide in the melt can unexpectedly give rise upon solidification to a variety of allotropic crystalline modifications [3].

3.2. Determination of the phase transition temperatures T^*_{cr} and T_g

Visual experiments in the optical cryostat have indicated that crystallization of the s.l. occurred between 200 and 250 K. Raman spectra measured every 2 K in this range have shown (Fig. 3) a superposition of the bands originating from both the s.l. and the crystalline solid (Fig. 1). By having a constant scattering geometry and fixed spectral conditions the intensities of the ~768, ~706 and ~680 cm^{-1} solid bands relatively to the intensities of the ~760 or the ~670 cm^{-1} bands of the s.l. could be measured at different temperatures in the 200–250 K range. The intensity vs. temperature plot gave S-type growth curves with increasing temperature for each band of the crystal. The derivatives of the S-type curves (see inset in Fig. 3) exhibit maxima at $T^*_{cr} = 233$ K, corresponding to the temperature of maximum crystallization speed, with an error of less than 2 K.

For the determination of the T_g, visual experiments were first carried out. The quenched melt gave at LN_2 a glass which formed by volume contraction a negative deep meniscus. At temperatures above 210 K it was observed that the meniscus started filling up with the s.l. and it was speculated that the T_g lays around this temperature. It was further observed that the strong polarized Raman band at ~780 cm^{-1} seen in the spectra of the glass, the s.l. liquid and the melt shifts appreciably with temperature. This is shown in Fig. 4 for a few temperatures while the inset of the same figure presents the frequency variation of this band at all temperatures where the spectra were measured for the amorphous phases. Below the 200–210 K region there is practically no change while at higher temperatures the peak frequency changes rather drastically with temperature. The origin of this change is discussed in the following section. As it has been observed in other glass forming systems abrupt changes occur around T_g for a variety of localized or delocalized vibrational modes of the glass/supercooled liquid. Examples are (a) the variation of the Boson frequency with temperature (see for example Refs. [10,11] for silicate glasses and Ref. [12] for zinc halide glasses) and (b) the variation of the 'stretching' fre-

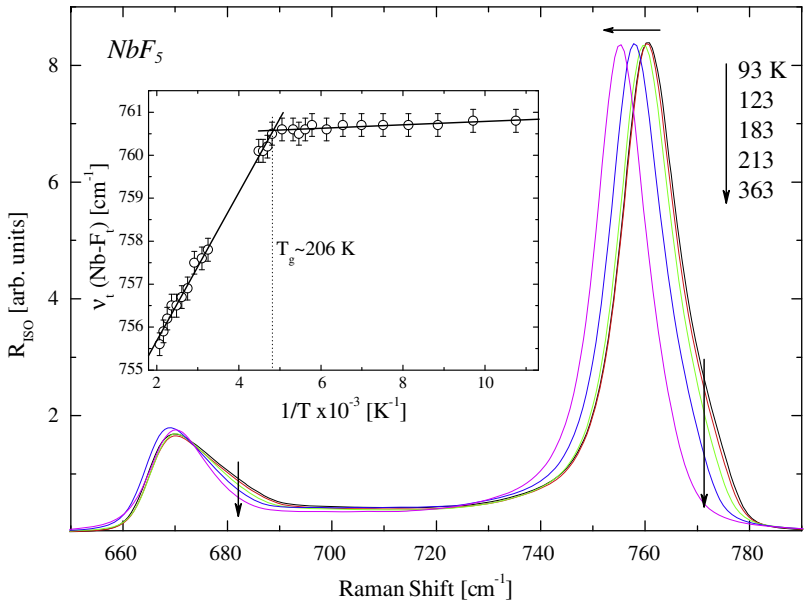

Fig. 4. Selected reduced isotropic spectra showing the temperature dependence of the "high" frequency Raman bands for the amorphous phases (glass, s.l., and melt). The vertical arrows show the intensity decrease of certain bands. Inset: variation of the Nb–F terminal frequency (ν_t) with the inverse temperature ($1/T$).

quency modes for oxide glasses like SiO_2 [10] and As_2O_3 [13]. In all these cases the frequency vs. $1/T$ plots are similar to that shown in Fig. 4 (inset) and the intersection of the two lines coincides with the calorimetric T_g of the system. In other words it is reasonable to use the intersection of the two lines in Fig. 4 to evaluate the glass transition temperature of the NbF_5. A value $T_g \approx 206 \pm 2$ K is obtained lying in the expected from the visual experiments T_g region. The very hygroscopic character of NbF_5 has prevented a reliable determination of the glass transition temperature with standard differential thermal analysis methods.

3.3. Estimation of the glass volume contraction

The visual/photographic experiments described in the Section 2 have shown that volume ratio of the s.liquid (V_l^*) and the glass (V_{gl}) is $V_l^*/V_{gl} \approx 1.2$. In other words the molar volume of the glass is contracted by ~17% relatively to the molar volume of the super-cooled liquid near T_g.

Volume contraction also occurred by super-cooling the melt from a temperature just above its melting point (~363 K) to room temperature (~300 K). A contraction of ~6 % was estimated which is very close to that calculated by extrapolating the density/temperature dependence equation which is measured for the liquid above its melting point [14].

4. Discussion

4.1. Vibrational/physicochemical properties and structure

Certain physicochemical properties of the NbF_5 phases are collected in Table 1. The vapor phase is characterized by a dimer (Nb_2F_{10})–monomer (NbF_5) equilibrium. The dimer (D) structure consists of two edge bridged octahedra (Fig. 5(a)) and its Raman spectrum (Fig. 1) is dominated by two 'high' frequency bands at 756 and 683 cm^{-1} which have been assigned to terminal (Nb–F_t) and bridging (Nb–F_b) frequencies, respectively [7]. A stretching frequency of the monomer (M) is also seen in the vapor Raman spectra whose intensity increases rapidly with increasing temperature due to the dimer dissociation [7].

The NbF_5 monoclinic crystal structure is made of isolated tetramers which are composed of four 'NbF_6' octahedra bound to each other by corners in a cis planar configuration (Fig. 5(b)) [9,15]. The highest strong Raman frequency of the solid at ~780 cm^{-1} (Fig. 1) has mainly been assigned to a Nb–F_t stretching mode [8]. The crystalline solid melts with rather high entropy of fusion and a molar volume increase by 31% [14]; properties indicating that drastic structural change occur during this phase transition. Furthermore, the melt viscosity and the Trouton's constant (Table 1) suggest the presence of highly associated species in the melt.

The Raman spectra of all the NbF_5 amorphous phases (glass, s.l. and melt) are rather 'isomorphous' indicating that the same basic scattering units are present in these phases. The spectra show a set of polarized bands in the high frequency region 650–800 cm^{-1} and a set of depolarized bands in the ~150–300 cm^{-1} re-

Table 1
Physiochemical properties of the NbF_5 phases [a]

Property [b]		Property [b]	
Crystal structure	C_{2h}^3–$C2/m$ monoclinic	ΔV_f	31%
Vapor structure [c]	Monomer–dimer equilibrium	ΔV_{gl} [d]	~17%
T_m [(K), °C]	352 (79)	η, at T_m (cp)	91.4
T_b [(K), °C]	507 (234)	σ, at m.p. (10^{-2} s m^{-1})	1.63×10^{-5}
ρ, Solid at 300 K (g cm^{-3})	3.54	ΔH_f (kJ mol^{-1})	13
ρ, Melt at m.p. (g cm^{-3})	2.697	ΔS_f (J K^{-1} mol^{-1})	34.5
T_g [d] [K, (°C)]	206 (−67)	Trouton's constant [e] (J K^{-1} mol^{-1})	102
T_{cr}^* [d] [K, (°C)]	233 (−40)		

[a] Data collected from Refs. [14,16].
[b] The symbols used are: T_m, melting point; T_b, boiling point; ρ, density; T_g, glass transition temperature; T_{cr}^*, crystallization temperature of the s.l.; $\Delta V_{gl} = 100(V_{m-l} - V_{gl})/V_{gl}$ the molar volume changes in the glass to s.l. transition; $\Delta V_f = 100(V_l - V_s)/V_s$, the molar volume change upon melting; η, viscosity; σ, specific conductance; ΔH_f, enthalpy of fusion ; ΔS_f, entropy of fusion.
[c] Ref. [7].
[d] This work.
[e] Trouton's constant corresponds to the entropy of vaporizations which for most liquids is ~85 J K^{-1} mol^{-1}.

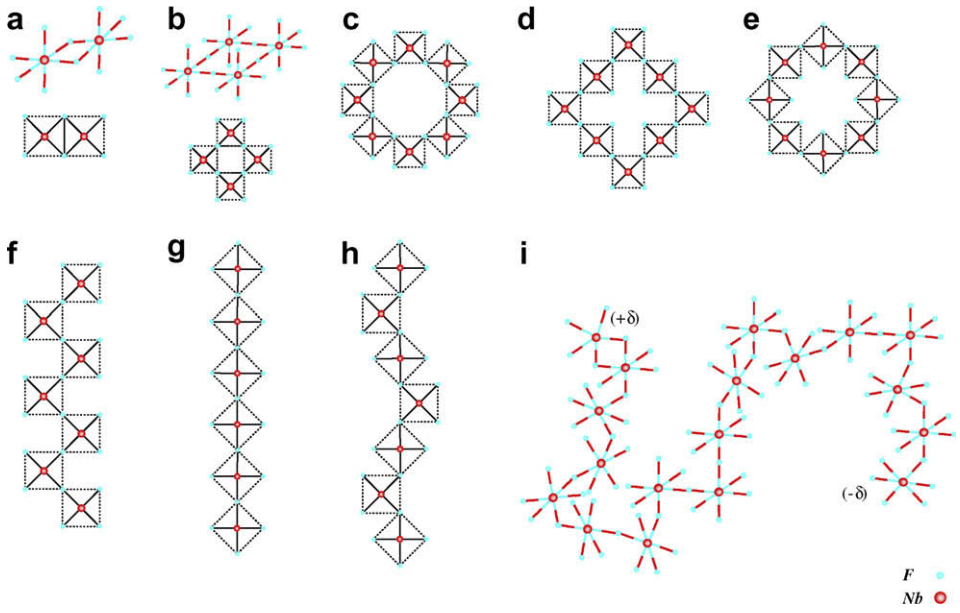

Fig. 5. Octahedra 'NbF_6' sharing either an edge or *cis* and/or *trans* vertices to form different structures. In most cases (two-dimensional projection) only the equatorial fluorides are shown at the vertices of the squares; the two axial fluorides are perpendicular above and below the central atom of the square and are not shown (a) edge-bridged dimer (found in the vapor phase, Ref. [7]); (b) cyclic tetramer, (found in solid NbF_5, Ref. [15]) only a *cis* configuration is possible; (c) *cis* cyclic octamer; (d) *trans* cyclic octamer; (e) mixed *cis/trans* cyclic octamer; (f) *cis* linear chain; (g) *trans* linear chain and (h) mixed *cis/trans* linear chain. Only a few cyclic structures and symmetric combination of linear chain structures are shown. Non-linear (space) structures can be easily formed by shifting the bridging vertex around the octahedra and thus creating complex 3D structures with random space orientation (i).

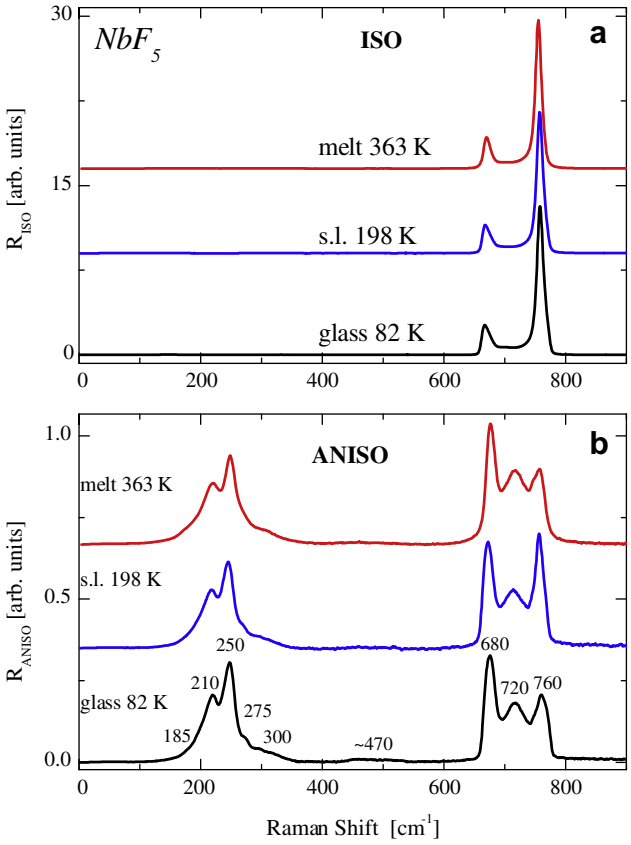

Fig. 6. Selected reduced isotropic (a) and anisotropic (b) Raman spectra of the amorphous phases. It should be noticed that the R_{ANISO} spectra are weaker than the R_{ISO} by a factor of 30.

gion. From the measured VV and VH spectra the reduced isotropic (ISO = VV − (4/3) VH) and anisotropic (ANISO = VH) representations [6] for all the amorphous phases have been calculated and shown in Fig. 6. The frequencies of the main Raman bands in the low temperature glass are marked on the spectra and listed in Table 2. With increasing temperature frequency shifts have been observed for certain Raman bands (see e.g. Fig. 4) but the overall spectra band intensities of the glass the s. liquid and the melt remain practically unchanged. The two intense ISO (polarized) bands of the amorphous phases have frequencies close to the two main frequencies of the dimer. A third rather weak ISO band is also present at ~140 cm^{-1}; this band can be easily seen in the expanded ISO spectra (inset) and in the VV spectra of Fig. 2(a).

In view of the absence of any structural information on the amorphous phases no definite assignments of the observed bands can be made. However, the proximity of the strong polarized bands of the amorphous phases to those bands corresponding to the terminal and bridging Nb–F frequencies of the gaseous dimer and to the terminal one of the tetramer in the solid, suggests that the bands at ~760 and ~660 cm^{-1} of the amorphous phases may arise from the Nb–F_t and Nb–F_b stretching frequencies, respectively. In other words, it is highly likely that the structure of the amorphous phases is dominated by 'NbF_6' octahedra bridged to each other by common fluorides. As it is well known from the crystal structures containing octahedral units, bridging occurs either in *cis* or *trans* configurations [9] thus, different combinations of bridging octahedra are expected to participate in the amorphous phase structure. Apart of the dimer and tetramer (Fig. 5(a) and (b)) other 'closed'

Table 2
Band frequencies of glassy NbF_5 at 82 K

Frequency (cm^{-1})	760 [b]	720	680[b]	660	(470)	
Characteristics [a]	p, s	dp, vw	dp, vw	p, s	dp, br, vw	
Frequency (cm^{-1})	(300)	(275)	250 [b]	210 [b]	(175) [b]	140
Characteristics [a]	dp, sh, vw	dp, sh, vw	dp, w	dp, w	dp, sh, vw	p, w

[a] p: polarized; dp: depolarized; s: strong intensity; w: weak; vw: very weak; br: broad band; sh: shoulder band.
[b] Also reported in Ref. [8].

structures like hexamers, octamers (Fig. 5(c–e)) etc or 'open' structures like chains (Fig. 5(f–h)) could also be formed by bridging 'NbF_6' octahedra. A mixture of these chain structures would give a perplex chain structure (i.e. Fig. 5(i)) containing three-dimensional branches which could also include, in part, 'closed' structures. The main characteristic of these structures is that each octahedron has *two bridged* fluorides to other octahedra and four, almost equivalent, *terminal* fluorides. This would imply that the terminal and bridging frequencies lay respectively in the same energy region for all these structures. In other words, when the 'NbF_6' octahedra with terminal and bridging fluorides are preserved in the amorphous phases, the frequency changes from configuration to configuration are expected to be small.

The two bridging fluorides for each octahedron can be either in a 'vis-à-vis' (*trans*) configuration (on 'line' as one extension of two axially bridged fluorides) or in a 'perpendicular' (*cis*) arrangement involving neighboring equatorial fluorides (Fig. 7; inset). These two bonding arrangements are expected to possess similar polarizabilities and hence to give rise to two – close in energy – bridging frequencies, i.e. $\nu_b^{(1)}$ and $\nu_b^{(2)}$. We suggest that the two bands resolved by Gaussian distribution analysis (Fig. 7) in the $\sim$670 cm^{-1} region (at $\sim$666 and $\sim$673 cm^{-1}) are associated with the two bridging components. Depending on the type of bridging, 'vis-à-vis' or 'perpendicular' three types of terminal fluorides are created. In the first case, four equivalent terminal fluorides on the equatorial plane are formed having a frequency $\nu_t^{(1)}$. On the other hand, in the 'perpendicular' arrangement two sets of equivalent terminal fluorides are formed with two fluorides disposed perpendicularly to the bridging plane and two laying on the bridging plane having frequencies $\nu_t^{(2)}$ and $\nu_t^{(3)}$, respectively. As seen in Fig. 7 the analysis of the terminal band near $\sim$760 cm^{-1} gives three Gaussian components (at $\sim$754, $\sim$785 and $\sim$768 cm^{-1}) which presumably arise from these three, close in energy, terminal frequencies. Finally, the resolved weak and broad band at $\sim$710 cm^{-1} is assigned to the bridging – breathing modes of the ring configurations participating in the structure. The broad ring size distribution expected in the glassy and liquid state is responsible for the large bandwidth of the 710 cm^{-1} mode. An interesting observation comes from Fig. 4 regarding the temperature dependence of the 768 cm^{-1} ($\nu_t^{(3)}$) and 673 cm^{-1} ($\nu_b^{(2)}$) band intensities. As illustrated from the inset in Fig. 7 both $\nu_t^{(3)}$ and $\nu_b^{(2)}$ are characteristic of the structure with the 'perpendicular' (*cis*) arrangement of the 'NbF_6' octahedra. The fact that both band intensities exhibit a systematic decrease with increasing temperature might imply a decrease in the number of closed structures where the 'perpendicular' arrangement of octahedral predominates.

The bridging configuration of 'NbF_6' octahedra ('chain' or 'ring' structures) determines the overall volume of the amorphous phases. The arrangement of the octahedra creates center voids in the ring structures and side voids in the chain structures; thus the large volume changes upon melting the solid (Table 1) can be justified by transforming the tetramers of the solid phase to extended ring structures or/and chain structures with large number of voids in the melt. In such a transformation the 'NbF_6' octahedra, are bridged in either *cis* and/or *trans* configurations without considerably changing their vibrational energies leading to almost constant terminal and bridging frequencies The basic units building up the amorphous phases are the vertex bridged 'NbF_6' octahedra which form a mixed network composed of chain and ring like structures. However, the volume contraction on going from the melt or the s.l. (Table 1) into the glass indicates that a more compact structure is formed in the glass by rearrangements of the shape and size of the chain and ring configurations, which lead to a decrease of center and side voids. As it is pointed out in Section 1 we have found that apart from NbF_5 there are other pentafluorides, with similar physicochemical properties, which formed glasses by quenching the melt to LN_2 temperatures. The liquid (melt) structure of one of them, the SbF_5, has been recently investigated by neutron and high-energy X-rays diffraction [17]. The data indicate that the liquid structure is predominated by *cis* bridged SbF_6 octahedra participating in tetramer (cyclic) and chain configurations. Our present and previous [4] proposed structures for the amorphous phases of NbF_5 and TaF_5 are in many respects compatible with the diffraction studies and modeling for SbF_5. In contrast the Raman data cannot exclude the presence of either larger then tetramers ring structures or/and *trans* bridging of the basic octahedral units in the chain configurations.

It seems that the measured physicochemical properties (Table 1) are in accordance with the proposed structural model. Furthermore, the similarities of the spectra for all amorphous phases suggest that the size of the cyclic and chain-like structures do not affect the ter-

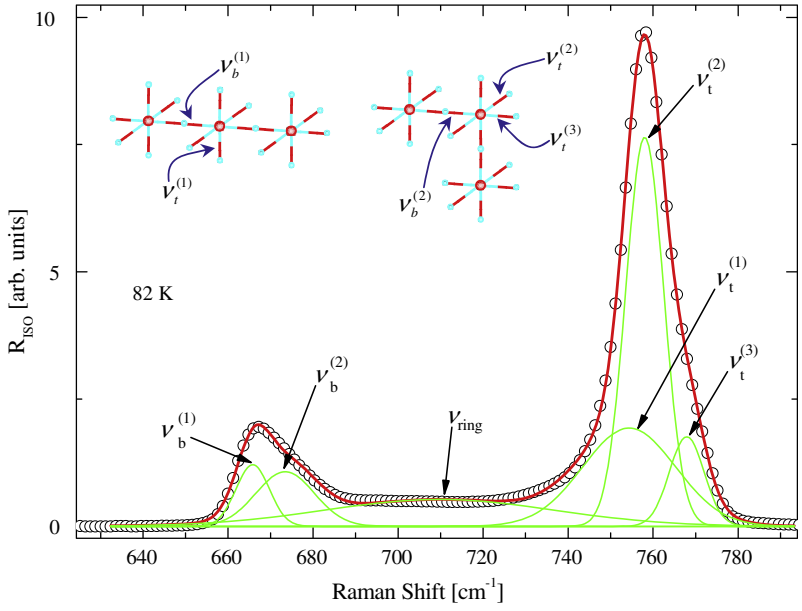

Fig. 7. Gaussian analysis of the terminal and bridging bands of the glass at $\sim$80 K. Inset: the two different bridging configurations of fluorides having the three Nb atoms in a '*vis a vis*' or a 'perpendicular' configuration.

minal and bridging frequencies of the basic octahedral 'NbF$_6$' units. The Raman spectra of molten NbF$_5$ measured at different temperatures are in support of this view (see also Figs. 4 and 6). Apart from an expected band broadening the spectra are practically independent of temperature; a fact that confirms the lack of a strong three-dimensional network structure, e.g. ZnCl$_2$ [3] and SiO$_2$ [10]. In the same temperature region the fluidity increases indicating structural changes (less polymerization; i.e. smaller rings, shorter chains) which do not change the vibrational modes of the 'octahedral' basic unit and thus do not alter the overall spectra. The small red shift of the ν_t with increasing temperature (Fig. 4) is probably due to the shortening of chains; a similar effect has been observed previously for the ZrF$_4$ – alkali fluoride melts [2].

Finally, it should be pointed out that the electrical conductivity of molten NbF$_5$ (Table 1) is two to three orders of magnitude higher that of the molecular melts like AlX$_3$ (X = Cl, Br) and very close to the conductivity of molten BeF$_2$ [16]. Thus, a small degree of 'ionization' is expected for the NbF$_5$ melt. The cyclic structures formed by the 'NbF$_6$' octahedra are more likely neutral and do not contribute to the conductivity. On the other hand, the chain structures have ending units, which could be charged either positively (e.g. a NbF$_5$ is edge or doubly bridged to the chain) or negatively (e.g. a NbF$_6$ octahedron is vertex bridged to the chain and possesses an additional terminal fluoride). By charging the chain endings (see ending units in Fig. 5(i)) one would expect that the melt should be slightly ionized and this is indeed what the specific conductance of the melt suggests (Table 1).

4.2. Low energy excitations: the Boson peak region

The low frequency peak situated at $\sim$10 cm^{-1} (see Fig. 2) is the well-known Boson peak which exists ubiquitously in the vibrational spectrum of any amorphous/glassy material. The Boson peak originates from non-Debye scattering mechanisms and is evident in Raman and inelastic neutron scattering. In particular, *excess* modes in the vibrational density of states (VDoS) $g(\nu)$ over the Debye behavior, $g^{\text{Debye}}(\nu) \propto \nu^2$ – which is characteristic of the vibrational density of states in a crystalline solid – are responsible for the appearance of the Boson peak [18]. It is important to notice that the Boson peak becomes evident in the frequency-reduced representation, $g(\nu)/g^{\text{Debye}}(\nu)$, while it does not appear as a distinct peak in $g(\nu)$ where it shows-up as a bump of small intensity. The use of the frequency-reduced representation has several shortcomings that have been summarized in Ref. [19], where analysis of experimental data for a number of glasses revealed that the spectral changes of the Boson peak under the application of external stimuli (temperature, pressure, etc.) can be understood by considering the corresponding dependence of the true excess of the VDoS, namely $g(\nu) - g^{\text{Debye}}(\nu)$.

The exceptionally low energy of the Boson peak, Ω^{BP}, in the NbF$_5$ glass indicates a very soft character of the vibrational modes. To our knowledge, Ω^{BP} of NbF$_5$ is the lowest one compared with other inorganic glasses whose values fall within the range 20–80 cm^{-1}. This is to be contrasted with the behavior of 'tetrahedral' strong, network-like glasses where the Boson peak remains well-resolved up to temperatures higher that the melting point [10,20]. The very low magnitude of Ω^{BP} for this glass as well as the relatively high value of the Boson peak anharmonicity ($d\Omega^{\text{BP}}/dT \approx -4.4 \times 10^{-2}$ cm^{-1} K^{-1}), see inset in Fig. 2(b), are factors responsible for the loss of Boson peak visibility at a temperature much below T_g. The spectral region of the Boson peak exhibits a rather depolarized character ($\rho \approx 0.55$) which is practically temperature independent.

The very low energy of the peak in the frequency-reduced representation, $g(\nu)/g^{\text{Debye}}(\nu)$, indicates also a rather low energy of the peak of the excess vibrational density of states $g(\nu) - g^{\text{Debye}}(\nu)$. Therefore, in the spirit of the Euclidean random matrix theory [21], the loss of visibility of the Boson peak is related to the features of the potential energy landscape. The shift of the spectrum of the excess modes in VDoS to negative frequencies occurs due to structure softening that takes place above some critical temperature T_c. The relevant changes of the topology of the potential energy landscape involve a merging of the inherent structures (local minima) with saddle points. At the phonon → saddle transition [21] – occurring when crossing T_c (moving upwards) – the excess VDoS crosses the zero energy point $\nu = 0$. As a result, the finite (non-zero) density of states at $\nu = 0$ exhibits a remarkable increase in the frequency-reduced VDoS, which blurs the sharpness of the peak initially seen at $T < T_c$. Because in NbF$_5$ glass this transition occurs at a rather low temperature, we deduce that the excess VDoS – that is responsible for the Boson peak – is dominated by 'vibrational' motions of floppy character. Therefore, librational and/or torsional motions of the structures shown in Fig. 5 are possible candidates for the structural origin of the Boson peak in this glass. The depolarized character of the Boson peak spectral region, as stated above, fits with this picture because such librational/torsional modes are expected to be rather depolarized.

5. Conclusions

The existence of a new, rather fragile, fluoride glass NbF5 is established and its glass transition (T_g = 206 K) and crystallization (T_{cr} = 233 K) temperatures are determined. Systematic Raman spectroscopic measurements clearly show that the basic units building up the structure of all phases of NbF$_5$ are the 'NbF$_6$' octahedra bridged to each other in *cis* and/or *trans* configurations. The glass and the liquid structures are formed by intermixing a variety of such bridged units in cyclic (closed) and/or in chain (open) arrangements. The proposed structures are compatible with the overall physicochemical properties of NbF$_5$ and give an account of the electrical conductivity of the melt. The observed Boson peak in the Raman spectra of the glass is rather unique since it appears at exceptionally low frequencies relative to other halide and oxide glasses. Its origin is attributed to librational and/or torsional motions of the bridged octahedra.

References

[1] I.D. Aggarwal, G. Lu (Eds.), Fluoride Glass and Fiber Optics, Academic Press, Inc, Boston, 1991.
[2] V. Dracopoulos, J. Vagelatos, G.N. Papatheodorou, J. Chem. Soc. Dalton Trans. (2001) 1117, and refs. therein.
[3] S.N. Yannopoulos, A.G. Kalampounias, A. Chrissanthopoulos, G.N. Papatheodorou, J. Chem. Phys. 118 (2003) 3197.
[4] G.N. Papatheodorou, S. Boghosian, in: R.A. Mantz, P.C. Trulove, H.C. De Long, G.R. Stafford, M. Hagiwara, D.A. Costa (Eds.), Proceeding of the XIV International Symposium on Molten Salts, vol. PV 2004-24, The Electrochemical Society Inc., Pennington, N.J., 2006, p. 294.
[5] T. Ostvold, E. Rytter, G.N. Papatheodorou, Polyhedron 5 (1986) 821.
[6] G.N. Papatheodorou, S.N. Yannopoulos, Light scattering from molten salts: structure and dynamics, in: M. Caune-Escard (Ed.), Molten Salts: From Fundamentals to Applications, NATO Science Series II, vol. 52, Kluwer Academic Publishers, Dordrecht, 2002, p. 47.
[7] S. Boghosian, E.A. Pavlatou, G.N. Papatheodorou, Vibrational Spect. 37 (2005) 133.
[8] I.R. Beattie, K.M.S. Livingston, G.A. Ozin, D.J. Reynolds, J. Chem. Soc. A (1969) 958.
[9] A.F. Wells, Structural Inorganic Chemistry, fifth ed., Oxford University Press, New York, 1984.
[10] A.G. Kalampounias, S.N. Yannopoulos, G.N. Papatheodorou, J. Chem. Phys. 124 (2006) 014504.
[11] A.G. Kalampounias, S.N. Yannopoulos, G.N. Papatheodorou, J. Chem. Phys. 125 (2006) 164502.
[12] S.N. Yannopoulos, A.G. Kalampounias, G.N. Papatheodorou, J. Non-Cryst. Solids 307 (2002) 142.
[13] G.N. Papatheodorou, S.A. Solin, Phys. Rev. B 13 (1976) 1741.

[14] D. Brown, The Chemistry of Niobium and Tantalum, in: J.C. Bailar, H.J. Emelous, R. Nyholm, A.F. Trotmal-Dichenson (Eds.), Comprehensive Inorganic Chemistry, vol. 3, Pergamon Press, Oxford, 1973.
[15] A.J. Edwards, J. Chem. Soc. (1964) 3714.
[16] G.J. Janz, Molten Salt Handbook, Academic Press, New York, 1967.
[17] S.E. McLain, A.K. Soper, J.J. Molaison, C.J. Benmore, M.R. Dolgos, L.L. Yarger, J.F.C. Turner, J. Mol. Liquids 131 (2007) 239.
[18] J. Jäckle, in: W.A. Phillips (Ed.), Amorphous Solids: Low-Temperature Properties, Springer, Berlin, 1981, p. 135.
[19] S.N. Yannopoulos, K.S. Andrikopoulos, G. Ruocco, J. Non-Cryst. Solids 352 (2006) 4541.
[20] A.G. Kalampounias, G.N. Papatheodorou, S.N. Yannopoulos, J. Non-Cryst. Solids 352 (2006) 4619.
[21] (a) T.S. Grigera, V. Martin-Mayor, G. Parisi, P. Verrocchio, Nature 422 (2003) 89;
(b) G. Parisi, J. Phys.: Condens. Matter 15 (2003) S765.